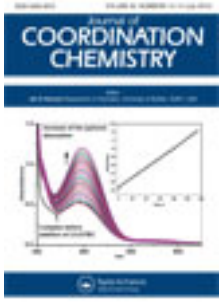

Journal of Coordination Chemistry
Publication details, including instructions for authors and subscription information:
http://www.tandfonline.com/loi/gcoo20

New mononuclear copper(I) and copper(II) complexes containing N_4 donors; crystal structure and catechol oxidase biomimetic catalytic activity

Abd El-Motaleb M. Ramadan [a], Mohamed M. Ibrahim [a b] & Ibrahim M. El-Mehasseb [a]

[a] Chemistry Department, Faculty of Science , Kafr El-Sheikh University , Kafr El-Sheikh 33516 , Egypt

[b] Chemistry Department, Faculty of Science , Taif University , Saudi Arabia

Accepted author version posted online: 03 May 2012.Published online: 22 May 2012.

To cite this article: Abd El-Motaleb M. Ramadan , Mohamed M. Ibrahim & Ibrahim M. El-Mehasseb (2012) New mononuclear copper(I) and copper(II) complexes containing N_4 donors; crystal structure and catechol oxidase biomimetic catalytic activity, Journal of Coordination Chemistry, 65:13, 2256-2279, DOI: 10.1080/00958972.2012.690513

To link to this article: http://dx.doi.org/10.1080/00958972.2012.690513

Journal of Coordination Chemistry
Vol. 65, No. 13, 10 July 2012, 2256–2279

New mononuclear copper(I) and copper(II) complexes containing N_4 donors; crystal structure and catechol oxidase biomimetic catalytic activity

ABD EL-MOTALEB M. RAMADAN*†, MOHAMED M. IBRAHIM†‡ and IBRAHIM M. EL-MEHASSEB†

†Chemistry Department, Faculty of Science, Kafr El-Sheikh University, Kafr El-Sheikh 33516, Egypt
‡Chemistry Department, Faculty of Science, Taif University, Saudi Arabia

(*Received 12 December 2011; in final form 20 March 2012*)

The synthesis of new tetradentate Schiff-base containing N_4 donors is described along with the preparation of a series of copper complexes derived from this ligand. These complexes have the form [CuLX]X′, $X = OH^-$, $X' = ClO_4^-$ (**1**) or $X = X' = Cl^-$ (**2**); and $[CuL]H_2O(ClO_4)_2$ (**3**), in addition to a copper(I) complex $[Cu_2L_2](ClO_4)_2$ (**4**). The synthesized compounds were spectroscopically characterized, showing the N_4 donor ligand. The single-crystal X-ray structural analysis of **4** demonstrated the dimeric structure and univalent copper. This dimer consists of $[CuL]_2^{2+}$, two uncoordinated ClO_4^-, and one acetonitrile. Each ligand is tetradentate *via* pyridyl and azomethine nitrogen atoms, providing a strongly distorted tetrahedron around copper(I) despite the pseudo-macrocyclic skeleton of the ligand. These complexes have been evaluated as functional model systems for catechol oxidase enzyme using 3,5-di-*tert*-butylcatechol (3,5-DTBC) as the test substrate. The catalytic performance of the air oxidation of 3,5-DTBC to the corresponding light absorbing 3,5-di-*tert*-butylquinone (3,5-DTBQ) at ambient conditions was studied using UV-Vis absorption spectra. Complex **4** exhibits the highest catalytic activity with turnover number of $33\,h^{-1}$. A kinetic treatment on the basis of the Michaelis–Menten model was applied. Correlation among reactivity, binding constants, electrochemical properties, and the geometry was determined. These correlations showed that the rate of oxidation is linearly correlated with the binding constants for the five coordinate **1** and **2**. The catalytic investigations demonstrate that geometrical effects are only one facet of the activity. The probable mechanistic implications of the catalyzed oxidation reactions are discussed.

Keywords: Crystal structure; Complexes; Biomimetic; Catalytic activity; Mononuclear; Catechol oxidase

1. Introduction

Binding and activation of small molecules like dioxygen under mild operating conditions by enzymatic systems and biomimetic complexes is a very active research field connecting the chemical synthesis and catalysis with technology [1–4]. In oxidative catalysis, transition metal complexes with polydentate Schiff bases are often used

*Corresponding author. Email: ramadanss@hotmail.com

ISSN 0095-8972 print/ISSN 1029-0389 online © 2012 Taylor & Francis
http://dx.doi.org/10.1080/00958972.2012.690513

featuring structural or functional properties of non-heme enzymes [5–7]. Copper is an essential bioelement for some time but its biological role(s) has been recognized only recently, a successful interaction between model complexes and protein biochemistry [8–10]. Copper-containing proteins are involved in various processes in living systems. The importance of copper ions as catalysts in both enzymatic [5] and non-enzymatic [11] systems is well known. Many copper proteins activate molecular oxygen, and the functions of these proteins are varied, serving as oxygen carriers (hemocyanin) [12, 13] or as catalysts in oxygenation (oxygenases) or oxidation (oxidases) reactions [14, 15].

Catechol oxidase, an enzyme ubiquitous in plants, insects, and crustaceans [16], is a type III copper protein containing a binuclear active site specializing in two-electron oxidation of a broad range of *o*-diphenols (catechols) to the highly reactive *o*-quinones [13, 17, 18] that auto-polymerize to produce melanin, which in turn guards damaged tissues against pathogens and insects among many of its protective functions [19]. Catechol melanin, the black pigment of plants (black banana and black sugar), is a polymeric product formed by oxidative polymerization of catechol. Melanin plays a role in the prevention of organism damage *in vivo* by absorption of ultraviolet light. Formation of melanin does not always proceed rapidly with tyrosinase. This slow formation accounts for sunburn of skin, which occurs when irradiation is faster than melanin formation. Some attempts have been reported to develop catalysts which either promote the formation of melanin or retard the multistage processes of oxidation [3]. The catechol oxidase enzyme thus plays an important role in disease resistance in mammalian, bacteria, fungi, and higher plants.

Understanding of the structural and functional aspects of catechol oxidase has been obtained through modeling studies [20]. Although several dinuclear copper complexes emulate the enzyme [21–24] both structurally and functionally, a great number of mononuclear copper complexes are known to exhibit significant catecholase activity [25–27]. The Cu $\cdots$ Cu distance in dinuclear copper complexes needs to be less than 5 Å for effective electron transfer during the catalytic process to display catecholase activity [28, 29] while a non-planar geometry around the metal center is necessary for mononuclear complexes to be active for catechol oxidation [30]. The catalytic activity of the mononuclear complexes can be tailored by varying the geometry and the steric interactions around copper, thus providing opportunities to probe the structure–activity relationship. Several mechanism and theoretical investigations have been reported for binuclear catechol oxidase models [31–33] while for mononuclear counterparts remain surprisingly rare [34a,b].

Toward our overall objective of obtaining a deeper understanding of chemical and biological oxidation processes, we began small molecule modeling studies to obtain insights about these reactions. We recently reported a series of cobalt(III) oxime complexes as models for ascorbic acid oxidase [35], a series of mononuclear copper(II) complexes as functional mimics of catechol oxidase [36], copper(II) complexes of tetradentate Schiff bases as functional models of tyrosinase [37], and a copper(II) complex of a sterically demanding ligand as a functional model for vitamin C oxidase [38]. Continuing this theme of research, we now design new functional mimics of catechol oxidase.

Coordination chemistry of copper(II) complexes with chelates incorporating pyridine and amine donors have relevance to histidine coordinated copper proteins such as blue copper proteins, hemocyanin, tyrosinase, and cytochrome C oxidase [39]. We describe here the synthesis and crystal structure of a series of mononuclear copper complexes

with a sterically demanding N_4 donor that exhibit catecholase-like activity by efficiently oxidizing 3,5-di-*tert*-buty1catehol (3,5-DTBC) to 3,5-di-*tert*-butylquinone (3,5-DTBQ) under ambient conditions using air as an oxidant to further understand structure *versus* reactivity correlation.

2. Experimental

2.1. *Materials*

6-Chloro-2-hydrazinepyridine was prepared according to the literature method [40]. All chemicals used were of analytical grade.

2.2. *Syntheses*

2.2.1. Synthesis of the tetradentate Schiff base bis(6-chloro-2-hydrazinopyridine) (L). A solution of 0.01 mole (870 µL) of diacetyl in 10 mL ethanol was added dropwise to 40 mL ethanolic solution of 0.02 mole (2.59 g) of 6-chloro-2-hydrazinepyridine. The reaction mixture was refluxed for 2 h and the contents cooled to room temperature. Yellowish white precipitate separated by filtration was washed with hot ethanol and dried in vacuum. This crude product was recrystallized from hot aqueous methanol yielding pure white crystals. Yield: 74%. Anal. Calcd for $C_{14}H_{14}N_6Cl_2$ [L, 337.21] (%): C, 49.87; H, 4.18; N, 24.92; Cl, 21.03. Found (%): C, 48.95; H, 4.22; N, 24.99; Cl, 20.92. ^{1}H NMR (DMSO-d_6): $\delta = 10.23$ (s, 2H, –NH), 7.69–6.84 (m, 6H, –PyH), and 2.18 ppm (s, 6H, $-CH_3$). ^{13}C-NMR (DMSO-d_6): 155.7, 149.1, 143.5, 117.2, and 107.9 (PyC), 151.3 ($C = N_{azomethine}$), and 12.6 ppm ($-CH_3$). FAB-Mass: $M^+ = 337$ (Supplementary material, S3). The suggested chemical formula of **L** was proved *via* the spectroscopic techniques including infrared (IR) spectra, ^{1}H NMR, and ^{13}C NMR {Supplementary material (S1a,b) and (S2)}.

2.2.2. [LCu(OH)](ClO$_4$) (1). A solution of **L** (337 mg, 1.0 mmol) in 10 mL absolute MeOH was added dropwise (over 30 min) to a solution of $Cu(ClO_4)_2 \cdot 6H_2O$ (444 mg, 1.2 mmol) in 10 mL MeOH. The resulting solution was stirred for 1 h at room temperature. A solution of 68 mg (1.2 mmol) of KOH in absolute MeOH (5 mL) was added with constant stirring. The reaction mixture was stirred for another 1 h at room temperature to form red precipitate, then was filtered off, washed several times and finally dried in vacuum over CaO. Yield: 0.48 g (77%).

2.2.3. [LCuCl]Cl (2). A solution of **L** (337 mg, 1.0 mmol) in 10 mL absolute MeOH was added dropwise (over 30 min) to a solution of $CuCl_2$ (161 mg, 1.2 mmol) in 10 mL MeOH. The resulting reaction mixture was stirred for 1 h at room temperature. The volume of the solution was reduced to 10 mL in vacuum and then allowed to stand at room temperature. Black crystals of **2** were obtained after 2 days. Yield: 0.34 g (71%) and the m/z $[M]^+$ of **2** is 617, (Supplementary material, S4).

2.2.4. [LCu](ClO$_4$)$_2$H$_2$O (3). A solution of **L** (337 mg, 1.0 mmol) in 10 mL absolute MeOH was added dropwise (over 30 min) to a solution of Cu(ClO$_4$)$_2 \cdot 6$H$_2$O (444 mg, 1.2 mmol) in 10 mL MeOH. The resulting reaction mixture was stirred for 1 h at room temperature. The volume of the solution was reduced to 10 mL in vacuum and then allowed to stand at room temperature. Yellow crystals of **3** were obtained after 2 days. Yield: 0.48 g (77%) and M^+ of **3** is 518 (Supplementary material, S4).

2.2.5. [LCu]$_2$(ClO$_4$)$_2$ (4). A solution of **L** (337 mg, 1.0 mmol) in 10 mL absolute MeOH was added dropwise (over 30 min) to a solution of Cu(ClO$_4$)$_2 \cdot 6$H$_2$O (444 mg, 1.2 mmol) in 10 mL MeOH. The resulting solution was stirred at 60°C for 2 h. The volume of the solution was reduced to 10 mL *in vacuo*, and then the produced collected by filtration and dried. A single colorless crystal suitable for X-ray crystallography was obtained by recrystallization in MeOH : MeCN (3 : 1) solution, followed by slow evaporation of this solution. Yield: 0.56 g (52%).

2.3. *Physical measurements*

IR spectra were recorded using KBr discs from 4000 to 200 cm^{-1} on a Unicam SP200 spectrophotometer. Electronic absorption spectra were obtained in methanol solution with a Shimadzu UV-240 spectrophotometer. Magnetic moments were measured by Gouy's method at room temperature. ^{1}H NMR spectra in DMSO-d$_6$ were obtained on a Jeol 200–MHz NMR spectrometer. ESR measurements of the polycrystalline samples at room temperature were made on a Varian E9 X-band spectrometer using a quartz Dewar vessel. All spectra were calibrated with DPPH ($g = 2.0027$). The specific conductance of the complexes was measured using freshly prepared 10^{-3} mol L^{-1} solutions in electrochemically pure MeOH or DMF at room temperature using a YSI Model 32 conductance meter. The thermogravimetric measurements were performed using a Shimadzu TG 50-Thermogravimetric analyzer from 25°C to 800°C under N_2. Elemental analyses (C, H, and N) were carried out at the Micro analytical Unit of Cairo University.

2.4. *Electrochemical measurements*

Cyclic voltammetric (CV) measurements were performed in a single compartment cell with a three electrode system on an EG & G PAR 250 potentiostat/galvanostat equipped with an IBM computer and a Hewlett-Packard 7440 A X–Y recorder. The working electrode was a platinum sphere (area 0.37 cm^2) and Ag/AgCl electrode as the reference. A platinum wire was used as the counter electrode. The supporting electrolyte used was 0.1 mol L^{-1} *n*-Bu$_4$NClO$_4$. The solvents used were sufficiently pure and the concentration of the complexes was 0.001 mol L^{-1}.

2.5. *X-ray crystallography*

X-ray measurements were made using a Bruker SMART APEX2 CCD/ Rigaku R-AXIS Spider IP area-detector diffractometer with Mo-Kα radiation ($\lambda = 0.71073$). Intensities were integrated from several series of exposures, each exposure covering

5/0.5 in ω, and the total data set being a hemisphere/sphere. Absorption corrections were applied, based on multiple and symmetry-equivalent measurements [41]. The structure was solved by direct methods/Patterson [42]. All non-hydrogen atoms were assigned anisotropic displacement parameters and refined without positional constraints. Hydrogen atoms were located in the electron density difference map, assigned isotropic displacement parameters, and refined without positional constraints or constrained to ideal geometries and refined with fixed isotropic displacement parameters. Refinement proceeded smoothly to give the residuals shown in table 1. Complex neutral-atom scattering factors were used.

2.6. *Determination of the binding constants*

Kinetic investigations for the substitution of OH^- or Cl^- as the fifth donor of **1** and **2**, respectively, by thiourea were performed in a 1 cm path length optical cell with UV-Vis spectral changes recorded for reaction of **1** and **2** ($0.0001\,mol\,L^{-1}$) with thiourea ($0.003\,mol\,L^{-1}$) in methanol at 296 K. Thiourea was selected as entering nucleophile since its high nucleophilicity prevents back reaction with coligands. The substitution reaction was followed spectrophotometrically by monitoring absorption changes at 365 and 530 nm. The kinetic trace for this reaction was recorded at 365 and 530 nm and the experimental points superimposed by best single-exponential fit according to equation (1). These ligand substitution reactions were studied under pseudo-first-order conditions by using at least a 10-fold excess of thiourea. All listed rate constants represent an average value of at least three kinetic runs under each experimental condition.

2.7. *Catechol oxidase biomimetic catalytic activity*

A mixture of 1.0 mL of 3,5-DTBC solution ($3.0 \times 10^{-2}\,mol\,L^{-1}$) in methanol and 1.0 mL of copper complex solution ($3.0 \times 10^{-4}\,mol\,L^{-1}$) in methanol was placed in a 1 cm path length optical cell containing 1.0 mL of methanol in a spectrophotometer. The final concentration of reaction mixture is catechol ($1.0 \times 10^{-2}\,mol\,L^{-1}$) and complex ($l.0 \times 10^{-4}\,mol\,L^{-1}$). The formation of 3,5-DTBQ was followed by observing the increase of quinone absorption at 400 nm. For each set of observations, a curve of concentration of 3,5-DTBQ formed (calculated by using corresponding ε value) *versus* time was plotted and initial rates were calculated by drawing a tangent to curve at $t = 0$ and finding its slope. After this initial fast phase, the average rate of reaction was

Table 1. Molecular formulae, elemental analyses, and physical properties of **1**–**4**.

		Λ ($\Omega^{-1}\,cm^2\,mol^{-1}$)		Found (%) (Calcd)			
Complex	Color	DMF	MeOH	C	H	N	M
1	Red	75.33	90.76	32.77(32.36)	3.13(3.27)	16.22(16.19)	12.82(12.24)
2	Black	83.16	98.77	35.33(35.47)	3.67(3.37)	17.44(17.74)	13.93(13.41)
3	Yellow	167.96	196.47	27.21(27.11)	2.45(2.90)	13.65(13.56)	10.32(10.25)
4	Colorless	150.07	187.31	33.97(33.45)	3.37(3.18)	16.61(16.74)	12.23(12.65)

also calculated. The experiment was repeated under two sets: (i) in the reaction mixture the concentration of catalyst was varied (2.5, 5, 10, 20, 30, and 40×10^{-4} mol L^{-1}) and concentration of DTBC was kept constant at 1.0×10^{-2} mol L^{-1}. (ii) Concentration of DTBC was varied (2.5, 5, 10, 20, 30, and 40×10^{-2} mol L^{-1}) and concentration of catalyst was kept fixed at 1.0×10^{-4} mol L^{-1}. For each set of data initial rates were calculated and graphs of rate *versus* concentration of catalyst and rate *versus* concentration of catechol were plotted.

3. Results and discussion

3.1. *General*

Interaction of copper(II) with the tetradentate Schiff base yielded a series of copper(II) complexes. The stoichiometry of the complexes has been established from analytical investigations as 1 : 1 and shows that the complexes can be represented as [CuLX]X′, where $X = OH^-$, $X' = ClO_4^-$ (**1**), $X = X' = Cl^-$ (**2**), $[CuL](ClO_4)_2 \cdot H_2O$ (**3**), and $[Cu_2L_2](ClO_4)_2$ (**4**). Complex **4** is obtained as colorless crystals suitable for X-ray crystallography, while the other complexes are colored microcrystals, **1** red, **2** black, and **3** yellow. Several attempts to obtain a single crystal of **1**–**3** suitable for X-ray crystallography failed. However, the analytical, spectroscopic, and magnetic data enable us to predict structures (scheme 1).

3.2. *Molar conductance*

Molar conductance of 0.001 mol L^{-1} solutions of **1**–**4** in DMF and MeOH are given in table 1. The hydrated complex (**3**) and $[Cu_2L_2](ClO_4)_2$ (**4**) are 1 : 2 electrolytes [43] with molar conductance values of 150.37–167.96 and 185.42–196.47 Ω^{-1} cm^2 mol^{-1} in DMF and MeOH, respectively. The molar conductance values of **1** and **2** were 73.33–83.75 in DMF and 90.75–97.77 Ω^{-1} cm^2 mol^{-1} in methanol, suggesting 1 : 1 electrolytes [43].

3.3. *IR spectra*

A comparison between the main vibrational bands of **L** in its free and coordinated form (Supplementary material, S1a) leads to the following observations: (i) for all the complexes the azomethine ν(C = N) undergoes a shift to lower wavenumbers as a consequence of coordination of nitrogen [44, 45]. (ii) The in-plane ring deformation band, δ(py) at 585–624 cm^{-1} in free ligand, shifts to higher energy upon complexation due to bonding through pyridyl nitrogen [44, 46]. The out-of-plane ring deformation band γ(py) at 401 cm^{-1} is difficult to assign in spectra of the complexes because $\nu(M–N_{Schiff})$ is present. (iii) The far-IR spectra of the complexes exhibit new bands at 412–440 cm^{-1}, characteristic of metal-nitrogen stretching vibration [47]. For **2** the coordinated chloride exhibits an absorption in the region associated with terminal chloride ligand [48].

The presence of coordinated hydroxide and crystalline water in **1** and **3**, respectively, is inferred from the broad band at 3597 and 3462 cm^{-1}, respectively, characteristic

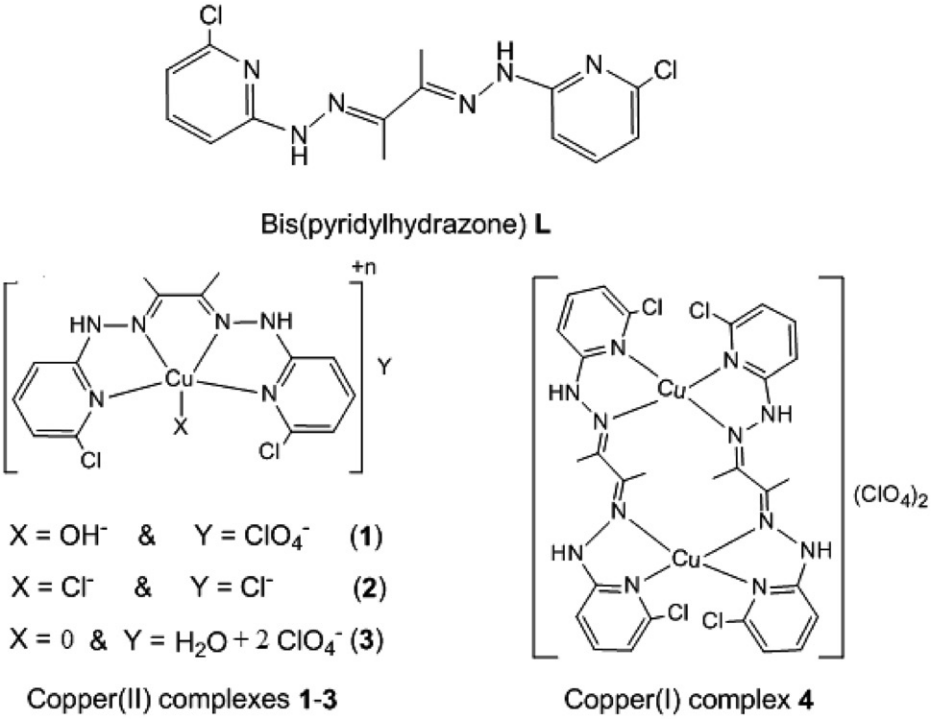

Scheme 1. The ligand **L** and its Cu(II) and C(I) complexes.

of ν(OH). The expected ν_3 and ν_4 IR bands of ClO_4^- with Td-symmetry are observed with splitting at 1100 and 657 cm^{-1} for **1**, 1100 and 625 cm^{-1} for **3**, and 1089 and 627 cm^{-1} for **4**, clearly revealing that ClO_4^- does not coordinate. Sharp and strong bands at 657 and 625 cm^{-1} indicate ionic ClO_4^- in all of these complexes [49, 50].

3.4. *^{1}H-NMR spectra*

The dimeric copper(I) complex, **4**, shows resolved ^{1}H-NMR spectrum in DMSO-d_6 at 400 MHz (Supplementary material, S5) confirming the diamagnetic character of copper(I) and supporting the reduction of copper(II) to copper(I) upon formation of the dimeric structure, confirming the dimeric formulation of **4**. ^{1}H-NMR data are consistent with, at least in solution, tetrahedral geometry of **4**.

3.5. *Electronic absorption spectra*

Electronic absorption spectra of the ligand and its copper(II) complexes **1**–**4** were measured at room temperature in DMF and methanol and the corresponding data are given in table 2. The spectrum of the free ligand has high energy absorption below 300 nm, due to pyridine $\pi \rightarrow \pi^*$ transition [51] and a strong absorption at 310 nm assignable to the $n \rightarrow \pi^*$ transition originating from the azomethine of the Schiff

Table 2. Electronic absorption spectra (cm^{-1}) of **1**–**4**.

Complex	$\pi \rightarrow \pi^*$ (py)	$n \rightarrow \pi^*$ C=N	d–d		
L	39,215	32,258			
1	35,037	27,571	12,658	14,705(sh)	
2	35,735	27,411	13,333	16,393(sh)	
3	36,461	28,850	$^2B_{1g} \rightarrow {}^2B_{2g}$	$^2B_{1g} \rightarrow {}^2A_{1g}$	$^2B_{1g} \rightarrow {}^2E_g$
4	35,739	27,996	14,919	17,456	19,632

Complex details are as listed in table 1.

base [52]. The absorption spectral data in table 2 show that there is a significant change in the energy of $\pi \rightarrow \pi^*$ and $n \rightarrow \pi^*$ bands on complexation. The band maximum in spectra of chelates shifts to lower frequencies relative to those in the free ligands. This bathochromic shift results from extended conjugation in the ligand forced by the chelated metal ion [53].

Electronic absorption spectra of five-coordinate copper(II) complexes fall into two general categories [54]. Square-pyramidal complexes typically show a high-energy absorption in the visible region with a low-energy shoulder. In contrast, trigonal-bipyramidal complexes have a low-energy absorption band with a high-energy shoulder in the visible region. As shown in table 2, the results are consistent with these criteria and the electronic spectra show visible absorption band maximum at 800 and 820 nm with a high energy shoulder at 610 and 650 nm for **1** and **2**, respectively. These spectral features of the d–d bands are consistent with coordination geometry close to trigonal bipyramidal [55] for copper(II) bound to four nitrogen atoms in addition to OH^- and Cl^- for **1** and **2**, respectively. This is further confirmed from results of ESR spectra. In contrast, the electronic spectrum of the hydrated four-coordinate **3** shows three d–d transitions at 790, 680, and 590 nm, unambiguously assigned to the three spin allowed transitions $^2B_{1g} \rightarrow {}^2B_{2g}$, $^2B_{1g} \rightarrow {}^2A_{1g}$, and $^2B_{1g} \rightarrow {}^2E_{1g}$, respectively [54, 56]. The band positions for **3** are comparable to those values reported for analogous complexes containing four-coordinate copper(II) in a square-planar structure [38, 57]. The spectrum of **4** in DMF exhibits intense UV absorption bands (table 2) due to the $\pi \rightarrow \pi^*$ and $n \rightarrow \pi^*$ transitions arising from pyridine and azomethine, respectively, but there is no absorption in the visible region, consistent with Cu(I).

3.6. *Magnetic studies*

The effective magnetic moments (BM) of the reported copper(II) complexes were measured at room temperature (table 3), which demonstrate that the copper(II) complexes are magnetically dilute [58] and the observed magnetic moments fall in the range 1.88–2.10 BM.

The X-band ESR spectra of polycrystalline samples of **1**–**3** were recorded at 9.1 GHz under the magnetic field strength 3100 G scan rate 1000 recorded at room temperature. Simulation of the obtained spectra indicates three different values of g, showing that copper(II) in five-coordinate complexes **1** and **2** is in a rhombically distorted ligand field. Complexes **1** and **2** show parameters which are characteristic of rhombic

Table 3. Magnetic moment values and ESR spectral data of **1**–**3**.

Complex	g_z	g_y	g_z	R	μ_{eff} (BM)
1	3.541	2.803	2.184	1.2	1.87
2	2.925	2.336	1.979	1.6	2.10
	$g_{\|\|}$	$g_\perp$	g_{av}	G	
3	2.463	2.110	2.227	4.209	1.93

Complex details are as listed in table 1.

symmetry. In contrast, trigonal-bipyramidal or tetragonal geometries involving compression of axial bonds would be consistent with these data [59, 60]. For systems with $g_z > g_y > g_x$ the parameter R ($R = g_z - g_y / g_y - g_x$) is a very useful. If the ground state is d_{Z^2} the value of R is greater than 1 and the stereochemistry of copper(II) ion is trigonal-bipyramidal; for the ground state being predominantly $d_{x^2-y^2}$ the value of R is less than 1. Complexes **1** and **2** show values of R (table 3) greater than 1, indicating five-coordinate, trigonal-bipyramidal geometry.

The spectrum of **3** gives the trend $g_{||} > g_\perp > g_e$ (2.0023), which supports that $d_{x^2-y^2}$ is the ground state [38, 57]. The observed g_{av} value (2.227) is less than 2.3 ($g_{av} = 1/3\, g_{||} + 2/3\, g_\perp$); consequently, the coordination environment is covalent in accord with the criterion of Kivelson and Neiman [61]. The G value (4.209) excluded any exchange interaction between the copper(II) centers for this complex in the solid state consistent with the results of magnetic moment measurements. However, these spectral features together with the position of the d–d absorption point to a square-planar structure where the equatorial plane is determined by four nitrogen atoms.

For **4**, in the EPR spectrum at room temperature no signals could be detected due to the diamagnetic copper(I), also supported from the highly resolved ^{1}H-NMR spectrum of **4** (Supplementary material, S3).

3.7. *X-ray structure analysis of [CuL]$_2$(ClO$_4$)$_2$*

Interactions of *bis*-(pyridylhydrazone) (**L**) with $Cu(ClO_4)_2 \cdot 6H_2O$ in a 1 : 1 molar ratio at 60°C afforded colorless crystals of $[CuL]_2(C1O_4)_2$ (**4**) with concomitant reduction of copper(II) to copper(I). The mechanism for reduction of copper(II) → copper(I) is not yet known. However, we believe that complex formation followed by reduction would be a plausible path for direct formation of the copper(I) complex, similar to the case reported [62]. The reduction may be ascribed to the fact that azomethine groups have a relatively high electron density on the donor nitrogen atoms as a result of significant induction effect of the two methyl groups within the carbonyl moieties. The lone pair of electrons in either a 2s or sp^2 hybridized orbital on trigonally hybridized nitrogen to acceptor orbitals on copper reduces the positive formal charge on copper(II), facilitating formation of copper(I) in the tetrahedral structure. Tetrahedral geometry of **4** is preferred by copper(I). Electronic properties of the donor nitrogen atoms of the Schiff-base, stereochemistries, and the dimeric nature of **4** play vital roles in reduction of Cu(II) to Cu(I). X-ray structural analysis indicates that the side pyridines are twisted to make a specific cavity around the imine N, which serves as a well-protected space for metal ions in low oxidation state.

Table 4. Crystal data and structure refinement of **4**.

Empirical formula	$C_{30}H_{31}N_{13}Cl_6O_8Cu_2$
Formula weight	1041.46
Temperature (K)	293(2)
Wavelength (Å)	0.71073
Crystal system	Orthorhombic
Crystal color	Colorless
Space group	*pnna*
Unit cell dimensions (Å, °)	
a	23.4272(9)
b	16.1408(5)
c	10.9994(3)
α	90
β	90
γ	90
Volume (Å^3), *Z*	4159.2(2), 4
Calculated density (g cm^{-3})	1.663
Absorption coefficient (mm^{-1})	1.472
F(000)	2104
Crystal size (mm^3)	$0.40 \times 0.30 \times 0.10$
θ range for data collection (°)	3.07–23.25
Limiting indices	$-25 \le h \le 26$; $-17 \le k \le 17$; $-12 \le l \le 12$
Reflections collected	5483
Independent reflections	2972 [R(int) = 0.0291]
Completeness to θ (°)	99.3
Data/restraints/parameters	2972/0/313
Refinement method	Full-matrix least-squares on F^2
Goodness-of-fit on F^2	1.024
Final R indices [$I > 2\sigma(I)$]	$R_1 = 0.0370$, $wR_2 = 0.0707$
R indices (all data)	$R_1 = 0.0600$, $wR_2 = 0.0784$
Largest difference peak and hole (e Å^{-3})	0.229 and −0.289

Complex **4** crystallized as a dimer in the orthorhombic crystal system in the space group *Pnna* (table 4). An ORTEP view of the structure of **4** is shown in figure 1. Selected bond lengths and angles are tabulated in table 5. The structure consists of a dimeric $[CuL]_2^{2+}$, two uncoordinated ClO_4^-, and one acetonitrile. The closest distance between Cu(I) and O of the perchlorates is ~4.38 Å. Each ligand is tetradentate *via* two nitrogen atoms to one copper and the other two nitrogen atoms to the other copper, providing a distorted tetrahedral arrangement about each copper(I). The dihedral angle between the two planes defined by the copper and the two chelate rings is *ca* 80°, appreciably smaller than the expected angle (89° between the two planes for a regular tetrahedral geometry). Similar distortion (dihedral angle 80.7°) has been observed for $[Cu(dmbp)]^+$ (dmpb = 6,6′-dimethyl-2,2′-bipyridine) [63]. The pyridine rings are not coplanar. The bond lengths are within the expected range for copper(I) complexes with Schiff-base ligands [64]. The Cu–Npy bond lengths are very similar to those found in typical four-coordinate copper(I) complexes [63, 65]. The Cu–$N_{azomethine}$ bonds (~2.033 Å) are slightly longer than Cu–Npy (~2.071 Å) bond lengths. The N–Cu–N angles ranging from 79.97° to 134.40° comprise the main distortion from the ideal tetrahedral shape. Thus, only minor deviations from planarity are found for the copper(I) coordination sphere in **4**. The distance between the two copper centers (4.33 Å) is too large for metal–metal interaction, but in the same range as that found in

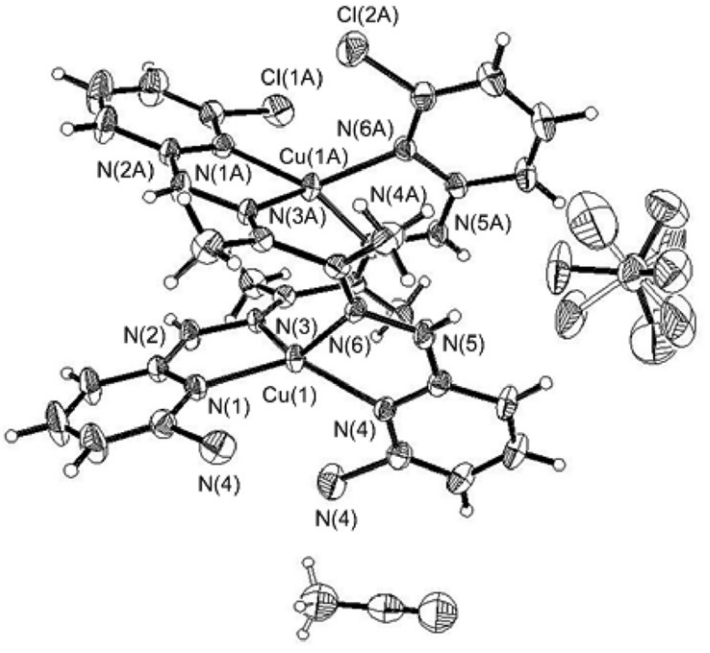

Figure 1. An ORTEP drawing of **4**. Ellipsoids are depicted at 30% probability.

Table 5. Selected bond lengths (Å) and angles (°) of **4**.

Cu(1)–N(1)	2.013(3)	N(1)–Cu(1)–N(6)	134.40(12)
Cu(1)–N(6)	2.033(3)	N(1)–Cu(1)–N(4)	125.22(11)
Cu(1)–N(4)	2.056(3)	N(6)–Cu(1)–N(4)	79.78(11)
Cu(1)–N(3)	2.086(2)	N(1)–Cu(1)–N(3)	79.97(10)
N(4)–N(5)	1.376(4)	N(6)–Cu(1)–N(3)	113.80(11)
N(5)–H(5)	0.790(3)	N(4)–Cu(1)–N(3)	130.94(10)
Cl(3)–O(1)	1.396(10)	(5)–N(2)–N(3)	118.9(3)
Cl(3)–O(2)	1.456(16)	C(5)–N(2)–H(2)	121(2)
Cl(3)–O(3)	1.398(11)	N(3)–N(2)–H(2)	120(2)
Cl(3)–O(4)	1.318(8)	C(6)–N(3)–N(2)	118.6(3)

other dimeric copper(I) complexes with tetrahedral arrangements [66–68] of 4.28–4.86 Å. A view of the packing of **4** is shown in figure 2 illustrating $\pi \cdots \pi$ interactions between pyridyl rings [67, 69].

3.8. *Electrochemical properties*

Electrochemistry of **1**–**3** was investigated, as the redox potential is an important parameter in electron transfer processes and in our catalytic systems. The reduction of Cu(II) by 3,5-DTBC and the reoxidation of Cu(I) by dioxygen are significant steps in the catalytic cycle. The redox potentials of **1**–**3** were measured by cyclic voltammetry (CV) at a working platinum electrode in methanol containing 0.1 mol L^{-1} tetrabutyl

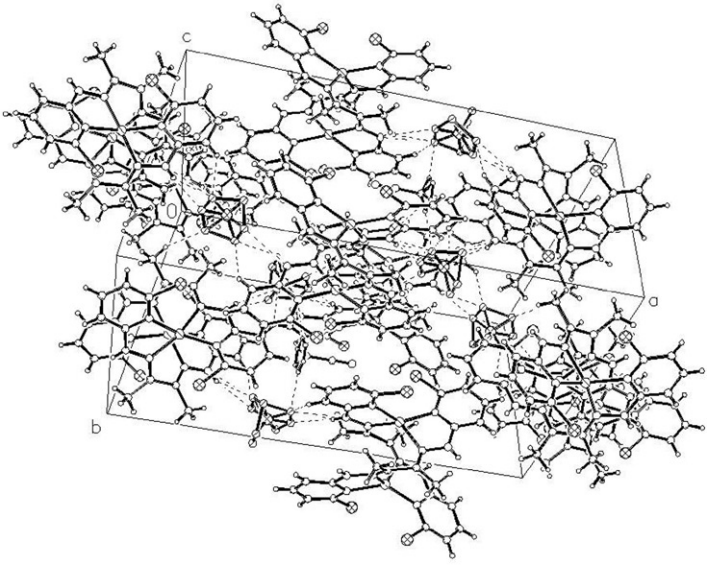

Figure 2. A packing diagram of **4**.

Table 6. Electrochemical data (mV) of **1**–**3**.

Complex	E_{pc}	E_{pa}	$E_{1/2}$	ΔE_p
1	390	450	420	60
2	388	355	424	72
3	415	480	447	65

Complex details are as listed in table 1.

ammonium perchlorate as the supporting electrolyte from 0.0 to 1.2 V *versus* AgCl/Ag. The CV data are given in table 6 and the cyclic voltammogram of **2** is shown in "Supplementary material", S6.

Complexes **1**–**3** exhibit a one-electron reduction at 0.393–0.410 V and the corresponding oxidation at 0.450–0.490 V. The electrochemical data, along with EPR results, establish that the complexes exist as monomers in solution. The reduced forms of **1**–**3** all display reasonable chemical stability on the time scale of the CV experiment. The complexes that undergo reduction are completely regenerated following electrochemical oxidation (the ratio of the peak currents i_a/i_c is about 1.0), suggesting a chemically reversible $Cu^{II} \rightleftharpoons Cu^{I}$ one-electron process. However, the value of the limiting peak-to-peak separation (ΔE_p), which lies within the normal values for a reversible one-electron redox process, suggests that the heterogeneous electron-transfer process in these complexes is easily reversible (ΔE_p, 60 mV for a reversible one-electron redox process) [70] and not accompanied by stereochemical reorganization [71]. The similarity in $E_{1/2}$ values for **1**–**3** show that the coordinating and electrolytic anions, OH^-, Cl^-, and ClO_4^-, have a negligible contribution on redox potentials. These redox potentials of **1**–**3**, however, do not differ greatly from the reported value of +360 mV *versus* SCE for the

enzyme tyrosinase isolated from mushrooms [72]. The impact of the electrochemical properties on the catalytic reactivity of these complexes will be discussed below.

3.9. *Determination of the binding constants*

The previously reported studies of copper(II) catecholase functional models demonstrated that exchange between the catecholate anion radical with one of the good leaving groups in the complex initiates the oxidation catalytic cycle. For five-coordinate copper(II) catecholase functional models, if the coordinating ligands are stronger than the catecholate anion, no oxidation will be observed. The fifth ligand must be released before coordination of catecholate to copper(II) and the association of oxygen during the catalytic oxidation cycle. To further elucidate the catecholase biomimetic catalytic activity of **1** and **2**, a detailed kinetic study on the labile fifth ligand (X), hydroxo and chloro, of **1** and **2** was carried out.

Kinetic studies were accomplished of X in [Cu^{II}(L)X] (X = OH, Cl) by thiourea (TU) as entering nucleophile. Thiourea was selected because of its high nucleophilicity that will prevent back reaction with X. The [Cu^{II}(L)X] (X = OH, Cl) complexes contain *bis*-imine and pyridine creating a strong π-acceptor that will increase the electrophilicity of the metal center [73, 74].

Reactions of [Cu^{II}(L)X] (X = OH, Cl) with thiourea were monitored kinetically from 250 to 600 nm. Solutions were prepared by dissolving known amounts of the appropriate complexes in methanol. The ligand-substitution reactions were studied as a function of TU concentration. An example of the UV-Vis spectral changes and a representative kinetic trace are presented in figure 3. Rate constants for the reactions were determined by using total TU concentrations of 0.001–0.01 mol L^{-1}, i.e. always at least in 10-fold excess over the copper(II) complex. Throughout the nucleophile concentration range it was possible to fit the absorbance/time traces to a one-exponential function by using equation (1).

$$Y = Y_o + Ae^{(-x/t)}. \quad (1)$$

This means that the overall reaction is monophasic, as shown in figure 3, for typical kinetic traces. Rate constant k_{obs} increases linearly with TU concentration (figure 4), which leads to second-order rate constant $k_2 = 17 \pm 2$ $(\text{mol L}^{-1})^{-1}\,\text{s}^{-1}$ for [Cu(L)Cl] and $0.5 \pm 0.1\,(\text{mol L}^{-1})^{-1}\,\text{s}^{-1}$ for [Cu(L)OH]. The rate constants demonstrate that substitution is slowed by a factor of 35 on going from the chloro to the hydroxo derivative.

3.10. *Catechol oxidase biomimetic catalytic activity studies*

The catechol oxidase biomimetic catalytic activity of copper complexes, as model systems, has been determined by catalytic oxidation of catechols [75a–d]. Among the different catechols used in catechol oxidase model studies, 3,5-DTBC is the most widely used substrate for catecholase activity of *tyrosinase* [76a,b]. Its low redox potential for the quinone-catechol couple makes it easy to be oxidized to the corresponding quinone 3,5-DTBQ, and its bulky substituents make further oxidation difficult. The product 3,5-DTBQ is stable and exhibits a strong absorption at $\lambda_{max} = 400$ nm ($\varepsilon = 1900\,(\text{mol L}^{-1})^{-1}\,\text{cm}^{-1}$ in MeOH) [77a]. Therefore, activities and reaction rates

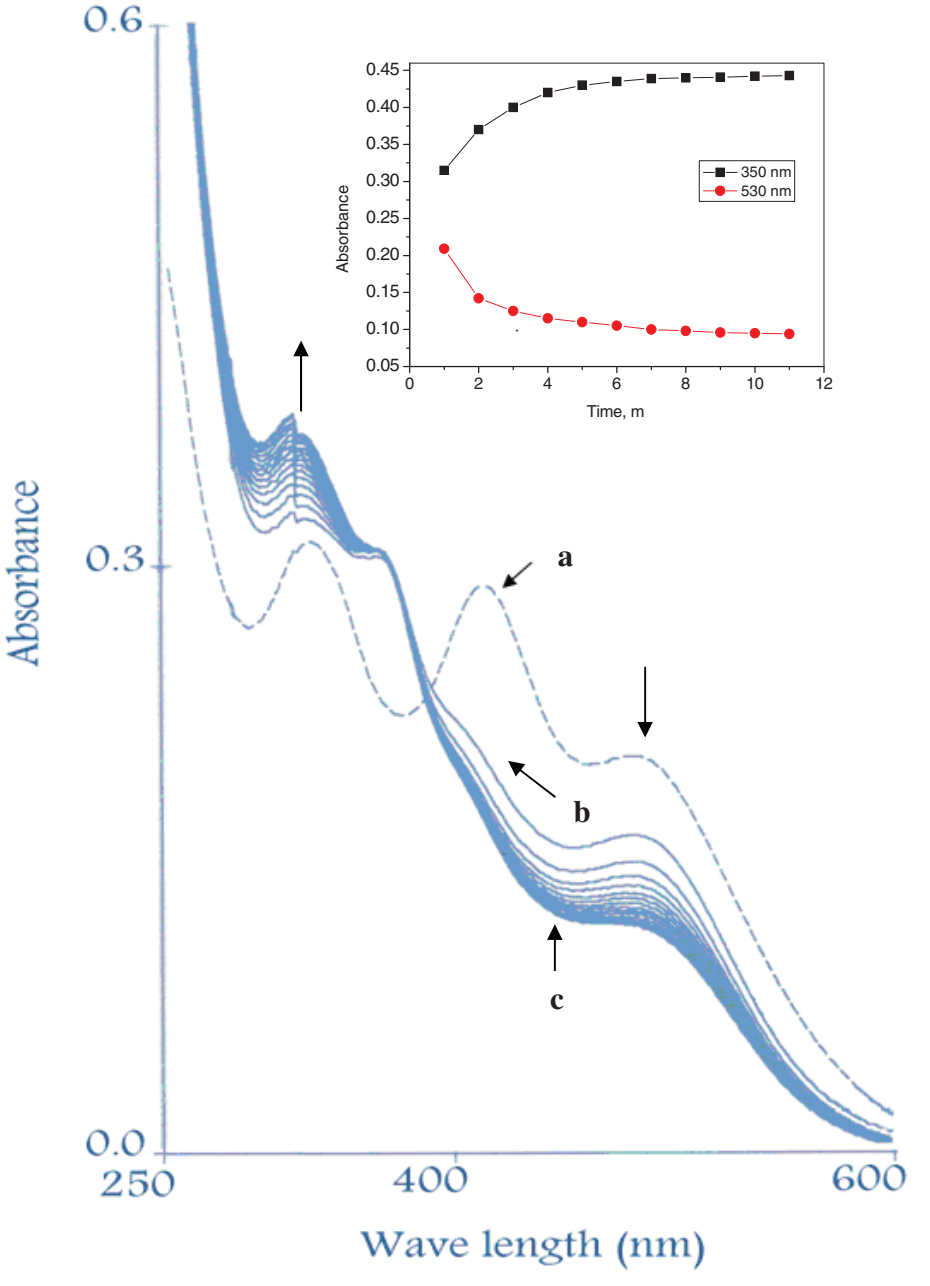

Figure 3. UV-Vis spectral changes recorded for the reaction of Cu(L)OH (1×10^{-4} mol L^{-1}) with thiourea (0.003 mol L^{-1}) in methanol at 296 K: (a) spectrum before the reaction; (b) spectrum obtained several minutes after mixing of the reactants; (c) at the end of the reaction in UV-Vis apparatus; Inset: typical kinetic trace recorded for this reaction at 350 and 530 nm. Experimental points superimposed by best single-exponential fit according equation (1).

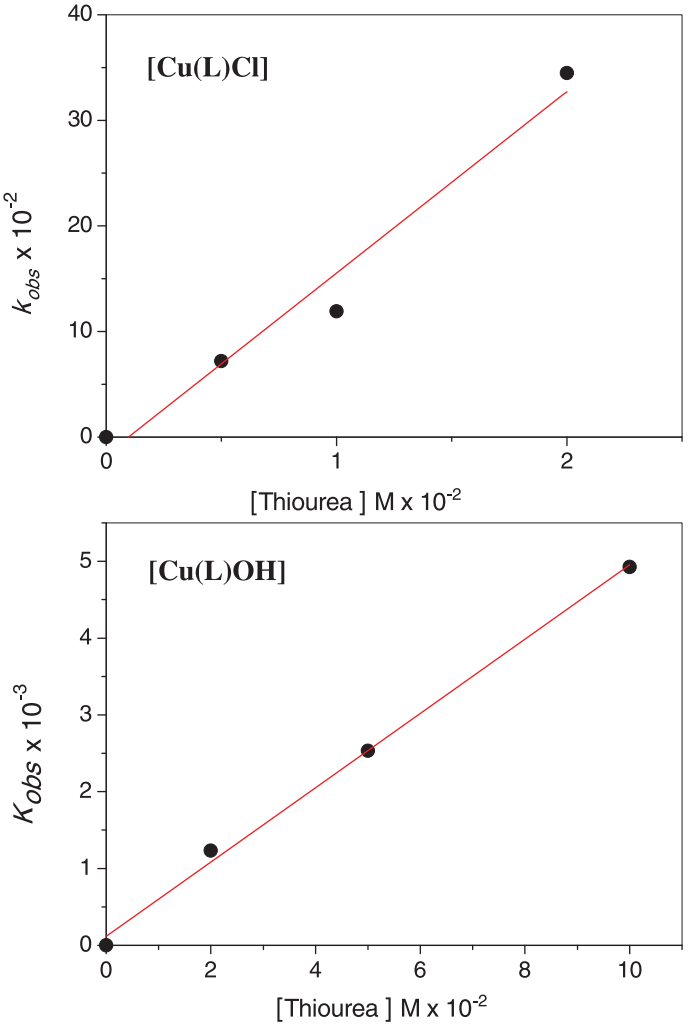

Figure 4. Plot of k_{obs} *vs.* thiourea concentration for [Cu(L)OH] and [Cu(L)Cl] in methanol at 296 K. Experimental conditions: [Complex] = 0.1 mmol L^{-1}, wavelength 350 nm.

can be determined using electronic spectroscopy by following the appearance of the characteristic absorption of 3,5-DTBQ. The reactivity studies were performed in methanol because of the solubility of the complexes as well as the substrate. When oxidation was allowed to continue for 48 h at room temperature, only *o*-quinone was detected. The exceptionally high stability found for *o*-quinone at room temperature suggests that a single reaction pathway is followed and that the *o*-quinone produced does not undergo further oxidative cleavage.

3.10.1. Initial rate studies. Prior to a detailed kinetic study, it is necessary to get an estimation of the ability of the complexes to oxidize catechol. The kinetic data were determined by initial rates, monitoring the growth at 400 nm of 3,5-DTBQ, formed due

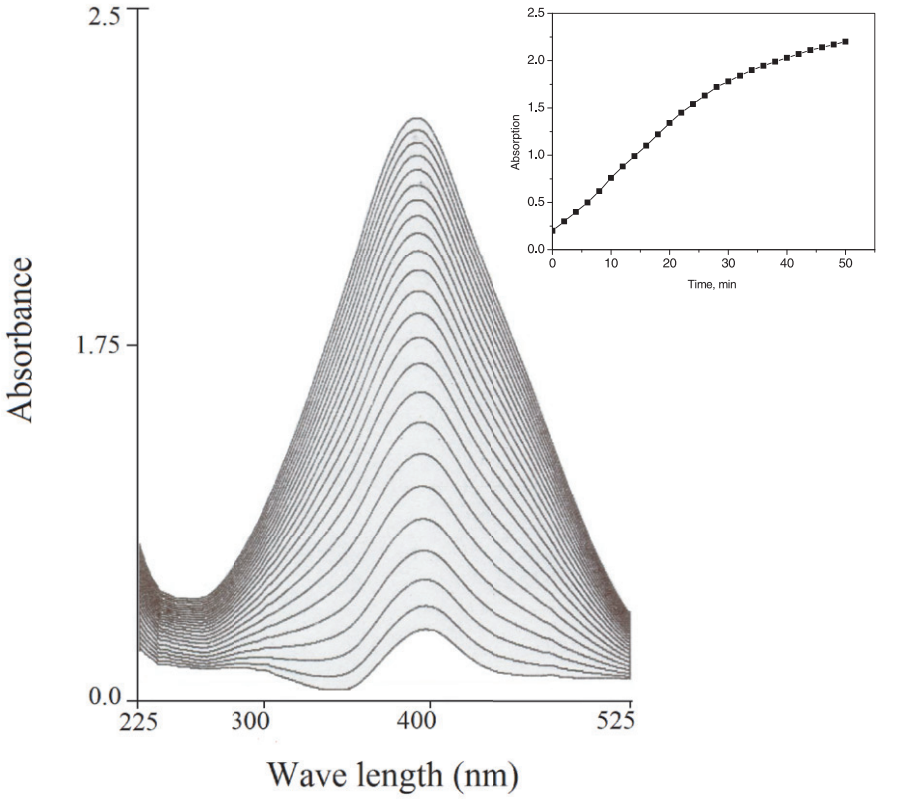

Figure 5. Time sequence of the increase in the absorption band of 3,5-DTBQ in oxidation of 3,5-DTBC ($0.01\ mol\ L^{-1}$) in the presence of **2** ($0.0001\ mol\ L^{-1}$) in methanol at 296 K; Inset: typical kinetic trace recorded for this reaction at 400 nm.

to oxidation of 3,5-DTBC in the presence of copper(II) complexes. Solutions ($1 \times 10^{-4}\ mol\ L^{-1}$) of **1**–**4** in methanol were treated with 100 equivalent of 3,5-DTBC in the presence of air. The absorbance was continually monitored at $\lambda = 400$ nm over the first 50 min; the data for **2** are presented in figure 5. Initial rates for **1**–**4** were determined from the slope of the tangent to the absorbance *versus* time curve at $t = 0$. Figure 5 shows the time course of the reaction of **2** with 5-DTBC. The first apparent result is that the reactivities of the complexes differ significantly from each other. The initial rate ($mol\ L^{-1}\ min^{-1}$) values are 5.48×10^{-4} (**1**), 17.62×10^{-4} (**2**), 2.37×10^{-4} (**3**), and 33.18×10^{-4} (**4**). Under identical conditions, without the presence of a catalyst, no significant quinone formation was observed. By comparison with other catechol oxidase model complexes, the reported models show high catecholase activity. The k_{cat} values of 21.00–171.96 h^{-1} (table 7) are comparable to those values recently reported for other model systems ($k_{cat} = 21.5$–$65.0\ h^{-1}$) [25, 34a,b], but significantly lower than those reported for binuclear copper complexes ($k_{cat} = 200$–6000), and at least many orders of magnitude less active than the enzyme (8250) itself [77b]. On the basis of the k_{cat} values, the binuclear complexes show higher reactivity than mononuclear complexes due to this

Table 7. Kinetic parameters (k_{cat}, K_m, V_{max}, and % Yield) in methanolic solution at 298 K for aerobic oxidation of 3,5-DTBC to 3,5-DTBQ.

Complex	k_{cat} (h^{-1})	$K_m \times 10^{-3}$ (mol L^{-1})	$V_{max} \times 10^{-4}$ (mol L^{-1} s^{-1})	% Yield
1	21.0 (±0.3)	10.0 (±0.1)	3.5 (±0.1)	31.57
2	88.2 (±0.6)	9.5 (±0.2)	14.7 (±0.1)	48.00
3	15.0 (±0.4)	10.0 (±0.1)	2.50 (±0.05)	24.21
4	172 (±2)	9.2 (±0.1)	28.7 (±0.1)	78.94

Complex details are as listed in table 1. Yield percentage was determined at concentrations of 0.001 and 0.00001 mol L^{-1} of 3,5-DTBC and catalyst, respectively.

mechanism requiring two metal ions in close proximity. Complex **4** displayed much superior activity than **1**, **2**, and **3**.

To determine the dependence of the rates on the substrate concentration, solutions of **1**–**4** were treated with increasing amounts of 3,5-DTBC. First-order dependence was observed at low concentrations of the substrate, whereas saturation kinetics was found for **1**–**4** at higher concentrations (figure 6). Treatment on the basis of the Michaelis–Menten model, originally developed for enzyme kinetics, was applied. The kinetic data obtained here can be explained if we invoke, along the line of Jager and co-workers [78], a pre-equilibrium between the complex and the substrate. The subsequent redox processes and the substitution of one quinone by a second substrate are irreversible (rate determining steps). Although a much more complicated mechanism may be involved, the results show this simple model to be sufficient for a kinetic description.

The dependence of the reaction rate on the catalyst concentration is illustrated in figure 7; at constant concentration of DTBC, O_2, and a variable amount of catalyst, the initial rate is linearly dependent on the square of the catalyst concentration. As the curves in figure 7 pass through the origin, i.e. without intercept, it can be stated that there is no measurable rate of oxidation in the absence of the catalyst. It has been reported earlier that for a single mononuclear complex, the rate of DTBC oxidation depends linearly on the square of the copper(II) complex concentration [76a] in accord with our results.

Based on the above kinetic and catalytic investigations a probable catalytic reaction sequence can be represented as follows:

$$3,5-\mathrm{DTBC} + 2\left[\mathrm{Cu^{II}LX}\right] \rightleftharpoons \left[3,5-\mathrm{DTBC}-\left(\mathrm{Cu^{II}L}\right)_2\right] + 2\mathrm{HX}, \quad (2)$$

$$\left[3,5-\mathrm{DTBC}-\left(\mathrm{Cu^{II}L}\right)_2\right] \rightarrow 2\left[\mathrm{Cu^{I}L}\right] + 3,5-\mathrm{DTBQ}, \quad (3)$$

$$2\left[\mathrm{Cu^{I}L}\right] + \mathrm{O_2} \rightarrow \left[\left(\mathrm{Cu^{II}L}\right)_2\mathrm{O_2}\right], \quad (4)$$

$$3,5-\mathrm{DTBC} + \left[\left(\mathrm{Cu^{II}L}\right)_2\mathrm{O_2}\right] \rightarrow \left[3,5-\mathrm{DTBC}-\left(\mathrm{Cu^{II}L}\right)_2\mathrm{O_2}\right] + 2\mathrm{H^+}, \quad (5)$$

$$\left[3,5-\mathrm{DTBC}-\left(\mathrm{Cu^{II}L}\right)_2\mathrm{O_2}\right] + 2\mathrm{H^+} \rightarrow \left[3,5-\mathrm{DTBC}-\left(\mathrm{Cu^{II}L}\right)_2(\mathrm{OH})_2\right], \quad (6)$$

$$\left[3,5-\mathrm{DTBC}-\left(\mathrm{Cu^{II}L}\right)_2(\mathrm{OH})_2\right] + 2\mathrm{HX} \rightarrow 3,5-\mathrm{DTBQ} + 2\left[\mathrm{Cu^{II}LX}\right] + 2\mathrm{H_2O}. \quad (7)$$

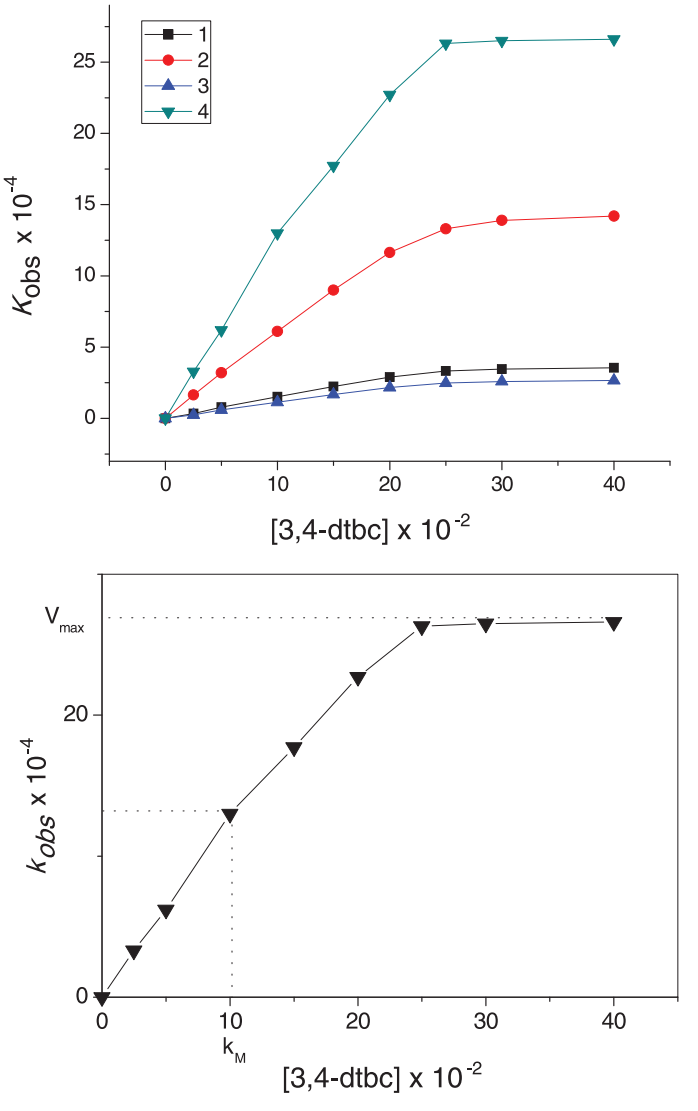

Figure 6. A comparison of the dependence of the reaction rates on 3,5-DTBC concentration for the aerial oxidation catalyzed by **4** (0.0001 mol L^{-1}) in methanol at 296 K.

For **1**–**3**, we believe that the non-protonated catecholate anion $DTBC^{2-}$ first binds to two molecules of the catalyst in a reversible pre-equilibrium step (equation (2)). The [catecholate-$(Cu^{II}L)_2$] intermediate oxidizes the coordinated catecholate anion (3,5-$DTBC^{2-}$) in a fast reaction to the corresponding light absorbing *o*-quinone (3,5-DTBQ) and forming the copper(I) species ($Cu^{I}L$) (equation (3)). Two molecules of this copper(I) complex then react in a reversible reaction with dioxygen in a slow, rate-determining step to give the copper dioxygen complex [$(Cu^{II}L)_2O_2$] (equation (4)). [$(Cu^{II}L)_2O_2$] reacts then with $DTBCH_2$ in fast reactions (equations (5)–(7)) to give

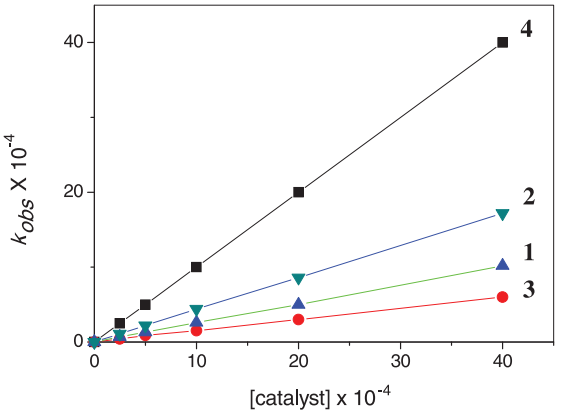

Figure 7. A comparison of the dependence of rates on catalyst concentration for aerial oxidation of 3,5-DTBC in methanol at 296 K and 3,5-DTBC = 0.001 mol L^{-1}.

DTBQ and two molecules of H_2O and the catalyst is regenerated in its original active form in closing up the catalytic cycle.

For **4**, the catalytic cycle is initiated with a mono anion catecholate bound $[Cu^{I}L]$ complex in a reversible pre-equilibrium step. Thereafter the [catecholate-$Cu^{I}L$] complex reacts with dioxygen in a further equilibrium step giving copper(II) superoxide complex [catecholate-$Cu^{II}LO_2$]. Prior investigation suggests the formation of a superoxide species in the catalytic cycle of catechol oxidase [25, 34, 79c]. The next step of the catalytic cycle involves a critical intramolecular proton transfer which occurs from the OH group of the catechol to the superoxide oxygen in [catecholate-$Cu^{II}LO_2$]. The intramolecular proton transfer in the superoxo species yielding a peroxo intermediate [catecholate-$Cu^{II}LO_2H$] is the overall rate-determining step of the catalytic cycle [25]. Similar proton transfer process has been suggested to be rate-determining in the catechol oxidation catalytic cycle [34]. Finally, the last step involves fast release of 3,5-DTBQ and H_2O_2 with concomitant regeneration of $[Cu^{I}L]$ to close up the reaction cycle (scheme 2). H_2O_2 would decompose to oxygen and water and more significantly, the disproportionation of H_2O_2 would render the catechol oxidation cycle thermodynamically favorable [25]. These mechanistic implications whereby $[Cu^{I}L]ClO_4$ (**4**) catalyzes the aerobic oxidation of 3,5-DTBC to 3,5-DTBQ are depicted in scheme 2.

Earlier work on oxidation of catechols by copper(II) complexes implicates both their structure features and electrochemical properties as important in determining the catalytic activity [79c]. For mononuclear five-coordinate copper(II) complexes with tetradentate ligands, changing the nature of the fifth donor has an effect on the rate of catalysis [78, 79a,b]. In this present study, a number of factors must be considered in assessing the differences in the catalytic reactivity of **1**–**4**. These include (i) the liability of the coordinated hydroxide or chloride incorporated in **1** and **2**, respectively, (ii) the electrochemical properties, and (iii) the geometrical considerations. All these factors will be considered sequentially.

3.10.2. Correlation with the binding constants. Several studies on catechol oxidation demonstrated that, for five-coordinate copper(II) complexes with tetradentate ligands, the degree of liability of the fifth ligand has an effect on the rate of catalysis [80].

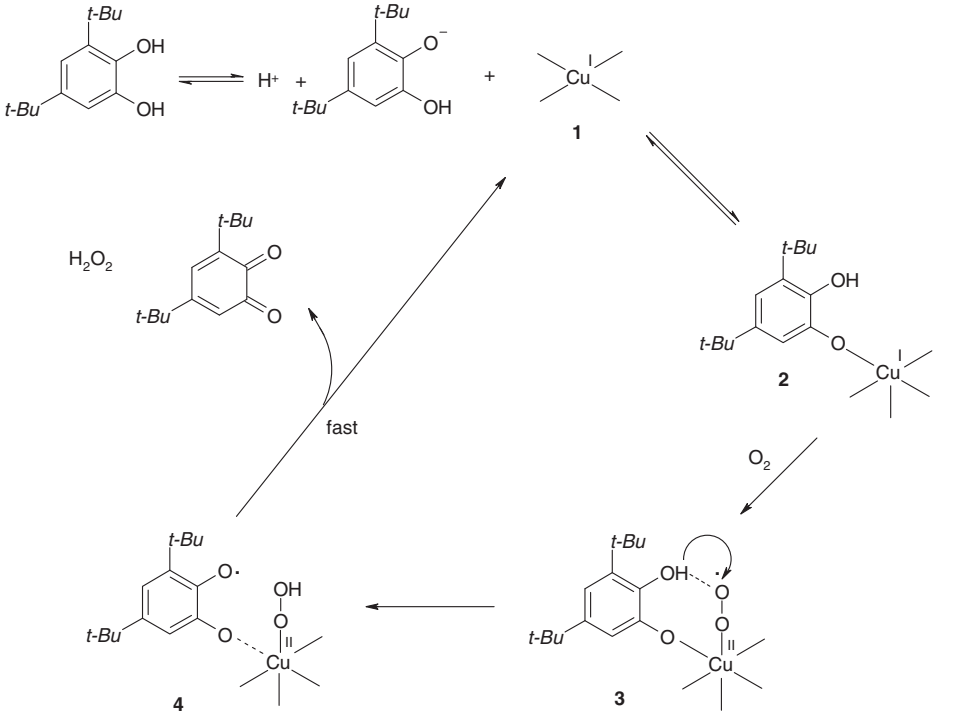

Scheme 2. Probable mechanism for aerobic catalytic oxidation of 3,5-DTBC in the presence of **4**.

In addition electron transfer from catechol to copper(II) can begin only after catechol and copper(II) form a copper(Il) catecholate intermediate [81]. Our premise is that the ease of dissociation of coordinated hydroxo or chloro of **1** and **2**, respectively, greatly affects the ability of the complexes to catalyze this oxidation. Although the five-coordinate **1** and **2** (containing tetradentate ligand) have a vacant coordination site, the possibility for binding the highly basic catecholate anion to copper(II) in [CuLX] seems remote because with excessive build up of the electron density on copper(II) and the Jahn–Teller effect, the resulting intermediate [catecholate–$(CuLX)_2$] is highly unstable. Dissociation of OH^- or Cl^- initiates oxidation. Therefore, the larger the binding constant for OH^- or Cl^- the slower the reaction will proceed. Binding constants of **1** and **2** to catalytic rates show a reasonable correlation (table 7). Kinetic study of ligand substitution of **1** and **2** demonstrated that liability of chloro is greater than hydroxo; the same order holds in their reaction with 3,5-DTBC. These results affirm that catecholase mimetic activity is dependent on the rate of dissociation of hydroxo or chloro. Reduction potentials are an important contributor to the catalytic properties of Cu(II) complexes [79, 80].

3.10.3. Correlation with the electrochemical properties. In oxidation of catechol to quinone the initiation step implies that Cu(II) is reduced to Cu(I) and subsequent reoxidation to Cu(II). The redox potentials ($E_{1/2}$) of **1**–**3** have been obtained to determine if there is a correlation between $E_{1/2}$ of these complexes and the rate of

oxidation of 3,5-DTBC. Several studies have shown previously that electrochemical potentials play a role in determining the reactivity of copper(II) complexes (although steric features of the ligands seem to be more important) [79, 80].

In assessing a correlation between redox potential and catalytic properties, no trend in these values is evident. It should be noted that the enzyme tyrosinase (catalyzes the aerobic oxidation of catechol to the light absorbing *o*-quinone) isolated from mushroom (*Agaricus bisporus*) has a reported value for E° of 0.36 V *versus* the standard calomel reference [72]. However, the enzyme balances the requirements of the different oxidation states of the metal in performing its catalytic tasks. The balance between ease of reduction of copper(II) and subsequent reoxidation copper(I) by molecular oxygen must be maintained for efficient catalysis. For **1** and **2** there was no obvious correlation between the redox potential and the reactivity, since **1** and **2** have redox potential values approaching the reported E° of the natural enzyme and the greater catalytic activity of **2** as compared to **1** is not correlated with its $E_{1/2}$. As observed by Malachowski and co-workers, the redox potentials display a secondary role in determining the reactivity of copper complexes [79, 80].

For **1** and **2**, redox properties are secondary to binding constants in determining the catalytic properties. From electrochemical values, the complex which is easiest to reduce and subsequently reoxidizes is also the one whose fifth ligand most easily dissociates.

3.10.4. Geometrical considerations. It has been stated that planar mononuclear copper(II) complexes are not active catalysts toward oxidation of catechols, presumably due to the lack of effective steric match between the substrate and the catalyst [81]. However, the results here show that square-planar **3** can be an effective catalyst and that geometrical effects are only one facet of the activity. Although five-coordinate trigonal bipyramidal (**1** and **2**) and tetrahedral **4** have redox potential values approaching the four-coordinate square planar **3** the latter exhibits lower reactivity, again suggesting the difference in reactivity of these chelates is not dependent only on electrochemical character of copper(II). Thus a possible explanation for the lower catecholase activity of **3** as compared to trigonal bipyramidal **1**, **2**, and the four coordinate tetrahedral **4** could be related to geometrical influence. It has been previously reported that a strong equatorial ligand field opposes the interaction of copper with a substrate, disfavoring formation of the intermediate copper-substrate adduct [82]. A strong field also disfavors reduction from copper(II) to copper(I) during the catalytic cycle. We suggest that coordination of the fifth ligand to copper(II) in trigonal bipyramidal complexes may reduce the strength of the equatorial field experienced by copper(II) as compared to square-planar complex. Another factor is the ability of the five-coordinate complex to change its geometry as the geometry of copper in the CuSOD enzyme also changes from square pyramidal [83]. This hypothesis finds support from Patel and co-workers who reported that higher SOD activity of five-coordinate copper(II) complexes is due to the presence of a fifth ligand in the axial position [84]. Interaction between the superoxide anion radical and copper(II) in five-coordinate geometry is induced due to the strong axial bond which results in increased catalytic activity [85].

The four-coordinate tetrahedral complex **4** is the most active catalyst while **1** and **2** are less reactive. These results for **1** and **2** suggest that their reactivity is decreased compared to **4** by the need for dissociation of the hydroxide or chloride.

4. Conclusion

A new tetradentate ligand containing N_4 donor sets and its mononuclear copper(II) **1**–**3**, and copper(I) **4** complexes were synthesized and characterized. The stereochemistries of these copper chelates vary between trigonal bipyramidal for **1** and **2** and square-planar for **3**. With the help of this ligand system, $[Cu(I)L]_2(ClO_4)_2$ was prepared and its structure determined. The magnetic measurements and the X-ray crystal structure of **4** show that copper(I) forms a distorted tetrahedron with the two ligand molecules in a dimeric formulation. These complexes catalyze the aerobic oxidation of 3,5-DTBC to 3,5-DTBQ at ambient conditions. No dioxygenase activities could be established. Kinetic studies reveal first-order dependence on catalyst concentration and saturation type behavior with respect to substrate. Dioxygenation of 3,5-DTBC did not take place, suggesting that this imine ligand prefers selectively oxidase-like activities of copper complexes. Geometry around copper, liability of the fifth ligand and electrochemical properties are factors that determine the catechol oxidase–mimetic catalytic activity of these complexes.

References

[1] L.I. Simandi. *Catalytic Activation of Dioxygen by Metal Complexes*, Kluwer Academic Publishers, Dordrecht (1992).
[2] J.S. Valentine, C.S. Foote, A. Greenberg, J.F. Liebman (Eds.). *Active Oxygen in Biochemistry*, Blackie, London (1995).
[3] J. Reedijk (Eds.), *Bioinorganic Catalysis*, Marcel Dekker, New York (1993).
[4] B. Meunier. *Chem. Rev.*, **92**, 1411 (1992).
[5] P.A. Vigato, S. Tamburini, D.E. Fenton. *Coord. Chem. Rev.*, **106**, 25 (1990).
[6] P. Guerriero, S. Tamburini, P.A. Vigato. *Coord. Chem. Rev.*, **139**, 17 (1995).
[7] J.S. Yamada. *Coord. Chem. Rev.*, **190–192**, 537 (1999).
[8] (a) M.C. Linder, C. Goode. *Biochemistry of Copper*, Plenum Press, New York (1991); (b) W. Kaim, J. Rail. *Angew. Chem. Int. Ed. Engl.*, **35**, 43 (1996); (c) T.N. Sorrel. *Tetrahedron*, **45**, 3 (1989); (d) N. Kitajima, Y. Morooka. *J. Chem. Soc., Dalton Trans.*, 2665 (1993).
[9] (a) N. Kitajima, Y. Morooka. *Chem. Rev.*, **94**, 737 (1994); (b) K.D. Karlin, J.D. Hayes, Y. Gultneh, R.W. Cruse, J.W. McKown, J.P. Hutchinson, J. Zubieta. *J. Am. Chem. Soc.*, **106**, 2121 (1984); (c) K.D. Karlin, Y. Gultneh, T. Nicholson, J. Zubieta. *Inorg. Chem.*, **24**, 3727 (1985).
[10] (a) R.R. Jacobson, Z. Tyeklar, A. Farooq, K.D. Karlin, S. Liu, J. Zubieta. *J. Am. Chem. Soc.*, **110**, 3690 (1988); (b) Z. Tyeklar, K.D. Karlin. *Acc. Chem. Res.*, **22**, 241 (1988).
[11] V. McKee, M. Zvagulis, V. Dagdigian, M.C. Path, C.A. Reed. *J. Am. Chem. Soc.*, **106**, 4765 (1984).
[12] K.A. Magnus, H. Ton, J.E. Carpenter. *Chem. Rev.*, **94**, 727 (1994).
[13] E.I. Solomon, M.J. Baldwin, M.D. Lowery. *Chem. Rev.*, **92**, 521 (1992).
[14] O. Hayaishi. *Oxygenases*, Academic Press, New York (1962).
[15] H. Sigel. *Metal Ions in Proteins*, Marcel Dekker, New York (1981).
[16] A.L. Hughes. *Immunogenetics*, **49**, 106 (1999).
[17] C. Gerdemann, C. Eicken, B. Krebs. *Acc. Chem. Res.*, **35**, 183 (2002).
[18] E.I. Solomon, U.M. Sundaram, T.E. Machonkin. *Chem. Rev.*, **96**, 2563 (1996).
[19] B.J. Deverall. *Nature*, **189**, 311 (1961).
[20] I.A. Koval, P. Gamez, C. Belle, K. Selmeczi, J. Reedijk. *Chem. Soc. Rev.*, **35**, 814 (2006).
[21] K. Selmeczi, M. Reglier, M. Giorgi, G. Speier. *Coord. Chem. Rev.*, **245**, 191 (2003).
[22] H. Borzel, P. Comba, H. Pritzkow. *Chem. Commun.*, 97 (2001).
[23] E. Monzani, G. Battaini, A. Perotti, L. Casella, M. Gullotti, L. Santagostini, G. Nardin, L. Randaccio, S. Geremia, P. Zanello, G. Opromolla. *Inorg. Chem.*, **38**, 5359 (1999).
[24] E. Monzani, L. Quinti, A. Perotti, L. Casella, M. Gullotti, L. Randaccio, S. Geremia, G. Nardin, P. Faleschini, G. Tabbi. *Inorg. Chem.*, **37**, 553 (1998).
[25] M.K. Panda, M.M. Shaikh, R. Butcher, P. Ghosh. *Inorg. Chim. Acta*, **372**, 145 (2011).
[26] G. Speier. *J. Mol. Catal.*, **37**, 259 (1986).
[27] Z.-F. Chen, Z.-R. Liao, D.-F. Li, W.-K. Li, X.-G. Meng. *J. Inorg. Biochem.*, **98**, 1315 (2004).

[28] R. Than, A.A. Feldman, B. Krebs. *Coord. Chem. Rev.*, **182**, 211 (1999).
[29] S. Kida, H. Okawa, Y. Nishida. In *Copper Coordination Chemistry: Biochemical and Inorganic Perspectives*, K.D. Karlin, J. Zubieta (Eds), p. 425, Adenine, Guilderland, NY (1983).
[30] N. Oishi, Y. Nishida, K. Ida, S. Kida. *Bull. Chem. Soc. Japan*, **53**, 2847 (1980).
[31] P.E.M. Siegbahn. *J. Biol. Inorg. Chem.*, **9**, 577 (2004).
[32] C. Eicken, B. Krebs, J.C. Sacchettini. *Curr. Opin. Struct. Biol.*, **9**, 677 (1999).
[33] T.R. Demmin, M.D. Swerdloff, M.M. Rogic. *J. Am. Chem. Soc.*, **103**, 5795 (1981).
[34] (a) A. Kupan, J. Kaizer, G. Speier, M. Giorgi, M. Reglier, F. Pollreisz. *J. Inorg. Biochem.*, **103**, 389 (2009); (b) J. Kaizer, T. Csay, G. Speier, M. Giorgi. *J. Mol. Catal. A: Chem.*, **329**, 71 (2010).
[35] A.M. Ramadan, S.Y. Shaban, M.M. Ibramim. *J. Coord. Chem.*, **64**, 3376 (2011).
[36] I.M. El-Mehasseb, A.M. Ramadan, R.M. Issa. *Trans. Met. Chem.*, **31**, 730 (2006), and references therein.
[37] A.M. Ramadan, M.M. Ibramim, S.Y. Shaban. *J. Mol. Struct.*, **1006**, 348 (2011).
[38] A.M. Ramadan, R.M. Issa. *Trans. Met. Chem.*, **30**, 471 (2005).
[39] (a) J.J. Frausto Da Silva, R.J.P. Williams. *The Biological Chemistry of the Elements – The Inorganic Chemistry of Life*, Oxford University Press, Clarendon, England (1991); (b) Z.L. Lu, C.Y. Duan, Y.P. Tian, X.Z. You, *Polyhedron*, **15**, 1769 (1996); (c) D.H. Busch, *Chem. Rev.*, **93**, 847 (1993).
[40] I. Buechi, P. Fabiani, H.V. Frey, A. Hofstetter, A. Schorno. *Helv. Chim. Acta*, **49**, 272 (1966).
[41] G.M. Sheldrick. *SADABS, Area-Detector Absorption Correction*, University of Göttingen, Germany (1996).
[42] G.M. Sheldrick. *Program SHELXS*, *Program for Crystal Structure Determination*, University of Göttingen, Germany (1997).
[43] W.J. Geary. *Coord. Chem. Rev.*, **7**, 81 (1971).
[44] A.M. Ramadan, I.M. El-Mehasseb. *Trans. Met. Chem.*, **23**, 183 (1998).
[45] R. Dilworth, C.A. McAuliffe, B.J. Sayle. *J. Chem. Soc., Dalton Trans.*, 849 (1977).
[46] R.J.H. Clark, C.S. Williams. *Inorg. Chem.*, **4**, 350 (1965).
[47] K. Nakamoto. *Infrared and Raman Spectra of Inorganic and Coordination Compounds*, 5th Edn, Wiley-Interscience, New York (1997).
[48] D.A. Waldwin, A.B.P. Lever, R.V. Parish. *Inorg. Chem.*, **10**, 107 (1971).
[49] M.M. Ibrahim, G.A.M. Mersal. *J. Inorg. Organomet. Polym.*, **19**, 549 (2009).
[50] G.B. Deacon, R.J. Phillips. *Coord. Chem. Rev.*, **33**, 227 (1980).
[51] K. Selmeczi, M. Reglier, M. Giorgi, G. Speier. *Coord. Chem. Rev.*, **245**, 191 (2003).
[52] (a) D.X. West, A.A. Nassar, F.A. EI-Saied, M.I. Ayad. *Trans. Met. Chem.*, **23**, 321 (1998); **23**, 423 (1998); (b) D.X. West, D.L. Huffman, J.S. Saleda, A.E. Liberta. *Trans. Met. Chem.*, **16**, 565 (1991); (c) D.X. West, I. Thientaravanich, A.E. Liberta. *Trans. Met. Chem.*, **20**, 303 (1995).
[53] K.Z. Ismail. *Trans. Met. Chem.*, **22**, 565 (1997); Z. Gang, C. Yuan. *Trans. Met. Chem.*, 19, 218 (1994).
[54] A.B.P. Lever. *Inorganic Electronic Spectroscopy*, Elsevier, Amsterdam (1970).
[55] B.J. Hathaway. In *Comprehensive Coordination Chemistry: The Synthesis, Reactions, Properties and Applications of Coordination Compounds*, G. Wilkinson, R.D. Gillard, J.A. McCleverty (Eds), Vol. 5, p. 533, Pergamon Press, Oxford (1987).
[56] K. Singh, M.S. Barwa, P. Tyagi. *Eur. J. Med. Chem.*, **42**, 394 (2007).
[57] M.M. Ibrahim, A.M. Ramadan, G.A.M. Mersal, S.A. El-Shazly. *J. Mol. Struct.*, **998**, 1 (2011).
[58] R.L. Dutla, A. Syamal. *Elements of Magnetochemistry*, 1st Edn, Affiliated East-West Press, New Delhi (2007).
[59] M.F. Cabral, R. Delgado. *Polyhedron*, **18**, 3479 (1999).
[60] B.J. Hathaway. *Coord. Chem. Rev.*, **52**, 87 (1983).
[61] D. Kivelson, R. Neiman. *J. Chem. Phys.*, **35**, 149 (1961).
[62] D. Datta, A. Chakravorty. *Inorg. Chem.*, **22**, 1085 (1983).
[63] P.J. Burke, D.R. McMillin, W.R. Robinson. *Inorg. Chem.*, **19**, 1211 (1980).
[64] B. Bordas, P. Sohar, G. Matolcsy, P. Berencsi. *J. Org. Chem.*, **37**, 1727 (1972).
[65] J.F. Dobson, B.E. Green, P.C. Healy, C.H.L. Kennard, C. Pakawatchai, A.H. White. *Aust. J. Chem.*, **37**, 649 (1984).
[66] M.M. Ibrahim, S.Y. Shaban. *Inorg. Chim. Acta*, **362**, 1471 (2009).
[67] M. Careri, L. Elviri, M. Lanfranchi, L. Marchiò, C. Mora, M.A. Pellinghelli. *Inorg. Chem.*, **42**, 2109 (2003).
[68] R. Cammi, M. Gennari, M. Giannetto, M. Lanfranchi, L. Marchiò, G. Morri, C. Paiola, M.A. Pellinghelli. *Inorg. Chem.*, **44**, 4333 (2005).
[69] M.M. Ibrahim, S.S. Gaied, M.M. Al-Qahtani. *Phosphorus, Sulfur, Silicon Relat. Elem.*, **185**, 2324 (2009).
[70] E.R. Brown, R.F. Large. In *Techniques of Chemistry: Physical Methods of Chemistry*, A. Weissberger, B. Rossiter (Eds.), Vol. 1, Part IIA, p. 475, Wiley, New York (1971).
[71] K.D. Karlin, P.L. Dahlstrom, J.R. Hyde, J. Zubieta. *J. Chem. Soc., Chem. Commun.*, 906 (1980).
[72] N. Makino, P. McMahill, H.S. Mason. *J. Biol. Chem.*, **249**, 6062 (1974).
[73] A. Hofmann, D. Jaganyi, O.Q. Munro, G. Liehr, R. van Eldik. *Inorg. Chem.*, **42**, 1688 (2003).
[74] S.Y. Shaban, F.W. Heinemann, R. van Eldik. *Eur. J. Inorg. Chem.*, 3111 (2009).

[75] (a) K. Selmeczi, M. Reglier, M. Giorgi, G. Speier. *Coord. Chem. Rev*., **245**, 191 (2003); (b) A. Neves, L.M. Rossi, A.J. Bortoluzzi, B. Szpoganicz, C. Wiezbicki, E. Schvingel. *Inorg. Chem*., **41**, 1788 (2002); (c) O. Seneque, M. Campion, B. Douziech, M. Giorgi, E. Riviere, Y. Journaux, Y.L. Mest, O. Reinaud. *Eur. J. Inorg. Chem*., 2007 (2002); (d) C. Belle, K. Selmeczi, S. Torelli, J.L. Pierre. *C.R. Chimie*, **10**, 1 (2007).
[76] (a) E. Monzani, L. Quinti, A. Perotti, L. Casella, M. Gulloti, L. Randaccio, S. Geremia, G. Nardin, P. Faleschini, G. Tabbi. *Inorg. Chem*., **37**, 553 (1998); (b) E. Monzani, G. Battaini, A. Perotti, L. Casella, M. Gullotti, L. Santagostini, G. Nardin, L. Randaccio, S. Geremia, P. Zanello, G. Opromolla. *Inorg. Chem*., **38**, 5359 (1999); (c) D. Bolus, G.S. Vigee. *Inorg. Chim. Acta*, **67**, 19 (1982); (d) F. Zippel, F. Ahlers, R. Werner, W. Haase, H.F. Nolting, B. Krebs. *Inorg. Chem*., **35**, 3409 (1996).
[77] (a) P. Gentschev, N. Moller, B. Krebs. *Inorg. Chim. Acta*, **300**, 442 (2000); (b) S.J. Smith, C.J. Noble, R.C. Palmer, G.R. Hanson, G. Schenk, L.R. Gahan, M.J. Riley. *J. Biol. Inorg. Chem*., **13**, 499 (2008).
[78] R. Wegner, M. Gottschaldt, H. Gorls, E.G. Jager, D. Klemm. *Chem. Eur. J*., **7**, 2143 (2001).
[79] (a) M.R. Malachowski, M.G. Davidson, J.N. Hoffman. *Inorg. Chim. Acta*, **157**, 91 (1989); (b) M.R. Malachowski, M.G. Davidson. *Inorg. Chim. Acta*, **162**, 199 (1989); (c) M.R. Malachowski, H.B. Huynh, L.J. Tomlinson, R.S. Kelly, J.W. Furbeejun. *J. Chem. Soc., Dalton Trans*., 31 (1995).
[80] (a) M.R. Malachowski, B.T. Dorsey, M.J. Parker, M.E. Adams, R.S. Kelly. *Polyhedron*, **17**, 1289 (1998); (b) M.R. Malachowski, B. Dorsey, J.G. Sackett, R.S. Kelly, A.L. Ferko, R.N. Hardin. *Inorg. Chim. Acta*, **249**, 85 (1996); (c) M.R. Malachowski, L.J. Tomlinson, M.G. Davidson, M.J. Hall. *J. Coord. Chem*., **25**, 171 (1992).
[81] M.M. Rogic, M.D. Swerdloff, T.R. Demmin. In *Copper Coordination Chemistry: Biochemical and Inorganic Perspectives*, K.D. Karlin, J. Zubieta (Eds), pp. 167–425, Adenine, Guilderland, NY (1983).
[82] R.P. Bonomo, E. Conte, R. Marcelli, A.M. Sontoro, G.J. Tabi. *J. Inorg. Biochem*., **53**, 172 (1994).
[83] (a) S.J. Lipard, A.R. Burger. K. Ugurbil, J.S. Valentine, W. Pantaliano, In *Bioinorganic Chemistry*, K.N. Raymond (Ed.), p. 251, American Chemical Society, Washington, DC (1977); (b) J.S. Richardson, D.C. Richardson, J.A. Trainer, E.D. Galtzoff. *Nature*, **306**, 284 (1986).
[84] R.N. Patel, N. Singh, K.K. Shukla, V.L.N. Gundla, U.K. Chauhan. *J. Inorg. Biochem*., **99**, 651 (2005); (b) R.N. Patel, N. Singh, K.K. Shukla, U.K. Chauhan, J.N. Gutierrez, A. Castineiras. *Inorg. Chim. Acta*, **357**, 2469 (2004).
[85] J.P. Collman, T.R. Halbert, K.S. Suslick. In *Metal Ion Activation of Dioxygen*, T.G. Spiro (Ed.), pp. 1–72, Wiley, New York (1980).